

## **Fast Fault Protection Based on Direction of Fault Current for the High-Surety Power-Supply System**

Li, Haijin; Chen, Min; Yang, Boping; Blaabjerg, Frede; Xu, Dehong

*Published in:*  
IEEE Transactions on Power Electronics

*DOI (link to publication from Publisher):*  
[10.1109/TPEL.2018.2870982](https://doi.org/10.1109/TPEL.2018.2870982)

*Publication date:*  
2019

*Document Version*  
Accepted author manuscript, peer reviewed version

[Link to publication from Aalborg University](#)

*Citation for published version (APA):*  
Li, H., Chen, M., Yang, B., Blaabjerg, F., & Xu, D. (2019). Fast Fault Protection Based on Direction of Fault Current for the High-Surety Power-Supply System. *IEEE Transactions on Power Electronics*, 34(6), 5787-5802. Article 8467349. <https://doi.org/10.1109/TPEL.2018.2870982>

### **General rights**

Copyright and moral rights for the publications made accessible in the public portal are retained by the authors and/or other copyright owners and it is a condition of accessing publications that users recognise and abide by the legal requirements associated with these rights.

- Users may download and print one copy of any publication from the public portal for the purpose of private study or research.
- You may not further distribute the material or use it for any profit-making activity or commercial gain
- You may freely distribute the URL identifying the publication in the public portal -

### **Take down policy**

If you believe that this document breaches copyright please contact us at [vbn@aub.aau.dk](mailto:vbn@aub.aau.dk) providing details, and we will remove access to the work immediately and investigate your claim.



# Fast Fault Protection Based on Direction of Fault Current for the High-Surety Power Supply System

Haijin Li, Min Chen, *Member, IEEE*, Boping Yang, Frede Blaabjerg, *Fellow, IEEE*, and Dehong Xu, *Fellow, IEEE*

**Abstract**—The high-surety power supply system, Super Uninterruptible Power Supply (Super-UPS), is an evolution of the traditional UPS. It consists of multiple sources, multiple energy storages and redundant power converters to improve the reliability of the power supply system significantly. In this paper, a fast fault protection scheme based on direction of fault current without the assistance of communication for Super-UPS is presented. It achieves fast and selective fault detection and ensures the uninterruptible load power when short-circuit faults occur. The directional fault current detection and the coordination between the circuit breakers and converters are investigated. The protection threshold setting are also discussed. In addition, an improved fault current measurement method, which can suppress the influence of stray inductance of the solid state circuit breaker, is presented to guarantee an accurate operation of the protection scheme for rapidly rising fault current. Finally, the proposed protection scheme and the improved fault current measurement method for Super-UPS are verified by experiments.

**Index Terms**—high-surety power supply, uninterruptible power supply, short-circuit fault protection, directional protection, solid-state circuit breaker

## I. INTRODUCTION

Uninterruptible Power Supplies (UPSs) have been widely used in Internet Data Centers (IDCs), telecommunications, factories, etc. Continuous and high-quality power is needed to guarantee the operation of critical loads during power faults due to the power aging, extreme weather or disasters. With the increasing amount of UPS capacity, the requirement of reliability also increases since the higher losses will be caused by the black-out. The concept of the high-surety power supply, namely Super-UPS, is proposed in [1]. It is an evolution of the traditional UPS. The architecture of a Super-UPS is shown in Fig. 1. It consists of multiple sources, multiple energy storages and redundant power converters to improve the reliability of the power supply system significantly. The solid-state circuit

breakers (SSCBs) are applied in the power conversion system to isolate short-circuit faults in the DC bus-side.

As shown in Fig. 1, all energy sources and storage components are connected to a common DC bus through power converters. Introducing multiple sources and storages brings challenges to protection of the power supply. If the short-circuit fault occurs in the bus side of a certain converter for energy sources or storage components, it will result in the collapse of the DC bus, which may cause interruption of power to the load. Therefore an effective fault protection strategy is necessary to isolate the faulty converter. Protection of Super-UPS may borrow the practices of the DC microgrid. However, Super-UPS seems to have a few specific characteristics to consider with respect to designing the protection. Firstly, Super-UPS is a compact system with lower line impedance ranging from a few to dozens of  $\mu\text{H}$ . Therefore the rising rate of fault current is very high. Besides, the reliability requirement for Super-UPS is much higher than general DC microgrids. For general DC microgrids, power outage time should be shorter than 10 ms according to the IEEE standard [2]. However, for Super-UPS, any short-time power interruption is unacceptable. Due to the high rising rate of fault current and uninterruptible power requirement, the requirement for protection speed and reliability is much higher in Super-UPS.

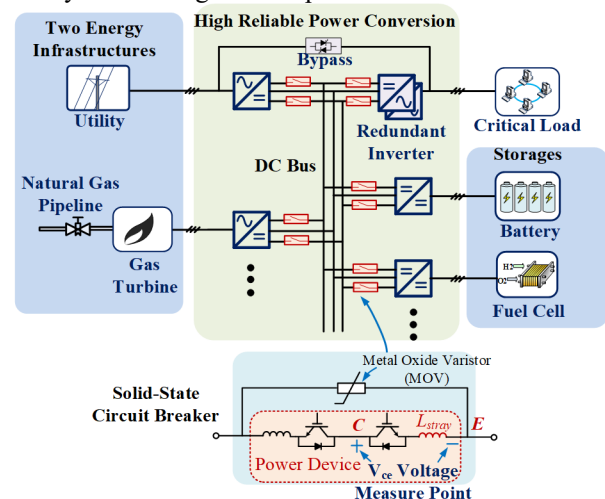


Fig. 1. The concept of Super-UPS with multiple power sources.

The protection of Super-UPS can be inspired by DC microgrids and DC zonal shipboard power systems. The protections of DC systems are investigated by previous works [8]–[28]. The conventional DC protection schemes and the brief comparison of different schemes are shown in TABLE I [8]–[29], [33]–[36]. The differential protection and directional comparison protection are communication-based protection

Manuscript received February 2, 2018; revised April 29, 2018 and July 27, 2018; accepted September 4, 2018. This work was supported by the National Natural Science Foundation of China (51337009). (Corresponding author: Min Chen, Dehong Xu)

H. Li, M. Chen, B. Yang and D. Xu are with the College of Electrical Engineering, Zhejiang University, Hangzhou 310027, Zhejiang, China. (e-mail: lihajin@zju.edu.cn; heaven@zju.edu.cn; tjuyangboping@126.com; xdh@cee.zju.edu.cn)

F. Blaabjerg is with the Department of Energy Technology, Aalborg University, Aalborg DK-9220, Denmark. (e-mail: fbl@et.aau.dk)

Color versions of one or more of the figures in this paper are available online at <http://ieeexplore.ieee.org>.

[17], [23], [26], [27], [36]. They are high accurate schemes with optimized selectivity. However, they highly depend on the communication. For the compact and high reliable power supply, Super-UPS, communication-based protections are not suitable because of the relatively slow protection speed. The distance protection, overcurrent protection, derivative protection and directional overcurrent protection are the non-communication based protection. The distance protection is not affected by operation conditions and short-circuit capacity [10], [22]. However, it is easily affected by the transient current and noises. It usually requires intense computing capabilities. For Super-UPS, due to the low line impedance of the power supply, the distance protection has low discriminability for the fault location. The overcurrent protection [19] and current derivative protection [20], [21], [24] can provide a fast fault detection, but they cannot achieve selectivity in the multiple-source system with bi-directional power flow such as Super-UPS. The directional overcurrent protection [35] is proposed to locate the feeder fault in the radial system with multiple sources. For Super-UPS, the directional overcurrent protection cannot achieve selectivity protection for all types of faults. In addition, the non-communication protection and communication-based protection are combined in [17], [33], [34]. In the combination scheme, the overcurrent protection is used to isolate the load or source fault quickly. The communication-based protection is applied to isolate bus faults. The protection speed is thereby improved. However, due to partially relying on the communication, it may cause temporary load interruptions in compact systems with fast increasing fault current. Thus, the existing methods cannot achieve uninterruptible load power with fast protection in Super-UPS. A fast and reliable, non-communication based, protection scheme is required for the Super-UPS.

In addition, for the protection methods based on the current detection, the measurement of rapidly rising high fault current is a big challenge in the compact system. Current measurement methods consist of current transformers (CTs), rogowski coils, Hall-Effect sensors, shunt resistors and the methods based on the voltage-drop of power devices [3]-[7], [23], [30]. The main challenge for CTs and rogowski coils is that DC component of current cannot be measured. The drawback of current shunt resistors is additional power losses [23]. The disadvantage of Hall-Effect sensors is the high cost. If solid-state circuit breakers are applied in the protection [3]-[7], the voltage drop of the power devices can be used to measure the fault current due to the low cost. However, the voltage drop of power device is affected by temperature. A temperature compensation method has been introduced in [7], [32]. Besides, the stray inductor of SSCBs, shown in Fig. 1, causes extra voltage drop on the measurement of  $V_{ce}$ . The measurement error is large when the derivative of the current is high. In order to achieve an accurate protection, the extra voltage drop caused by the stray inductor of SSCB should be extracted and compensated. The current measurement method with compensation of the influence of stray inductance is studied in this paper.

In this paper, a fast and reliable protection scheme is proposed for Super-UPS, which is a compact and high-surety power supply. The scheme achieves fast fault detection based on direction of current, and coordinates with converters to

ensure the uninterruptible load power. It does not rely on any communication. The protection speed and system reliability are improved. Then, an improved fault current measurement method is presented. The method eliminates the influence of stray inductance of SSCB on the measurement of the rapidly rising fault current. The accuracy of the protection scheme is also improved.

The rest of the paper is organized as follows. In Section II, a fault model is built, and the characteristic of fault current direction is analyzed. In Section III, a fast protection scheme based on the direction of fault current is developed. In addition, an improved measurement method for rapidly rising fault current is introduced. In Section IV, the prototype of Super-UPS is built, and experimental results are provided. Finally, the conclusions are given in Section V.

TABLE I  
COMPARISON OF DIFFERENT PROTECTION SCHEMES

Method	Merit	Shortcoming
Overcurrent Protection	Fast, reliable	Low selectivity
Current Derivative Protection	Fast, low current threshold	Sensitive to noises and system parameters
Distance protection	Not affected by operation conditions and short-circuit capacity	Sensitive to transient current and noises
Directional Overcurrent Protection	Selectivity for bi-directional power flow systems	Only suitable for radial systems
Directional Comparison Protection	High selectivity	Depends on the low bandwidth communication
Differential Protection	High selectivity, detects high impedance faults	Depends on the high bandwidth communication

## II. FAULT MODEL AND ANALYSIS OF SUPER-UPS

### A. Fault Types of Super-UPS

The architecture of Super-UPS can be considered as a single-bus radial system. The protection zones in Super-UPS can be divided into module protection zones and the bus-bar protection zone, which are shown in Fig. 2. In this section, the module fault is analyzed in detail.

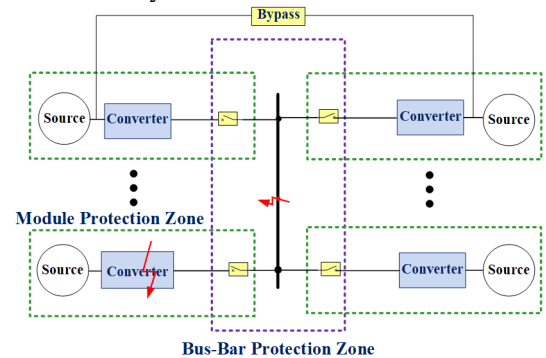


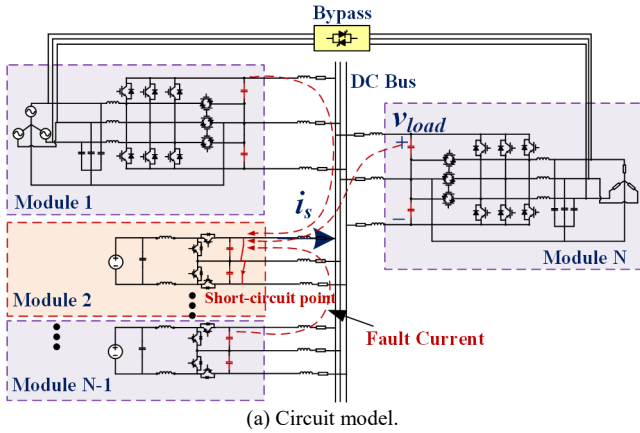
Fig. 2. The protection zones in Super-UPS.

The DC bus of a Super-UPS has three poles including a positive pole, a neutral pole and a negative pole. There are four short-circuit fault types of the module fault. They are positive pole short-circuited with negative pole, positive pole short-circuited with neutral pole, negative pole short-circuited with neutral pole and all three poles short-circuited together.

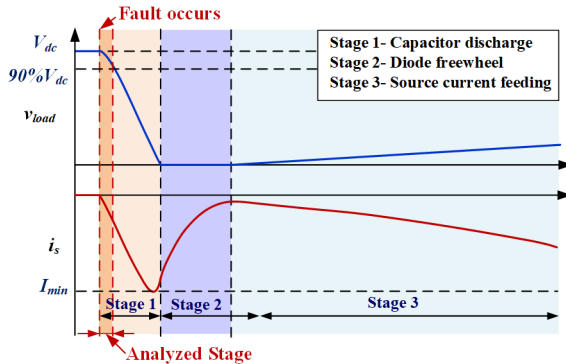
### B. Simplified Fault Model

The circuit model of a Super-UPS is shown in Fig. 3(a). The topologies with neutral point of DC bus are chosen due to the requirement of UPS. In UPS systems, the load inverter is required to provide the power for the unbalanced three-phase load, thus the DC bus needs the neutral point for the three-phase four-wire inverter. All energy sources and storage components are connected to a common DC bus through DC/DC or AC/DC converters. Since capacitors are installed in the DC port of converters, it results in the discharge current of the capacitors when the fault occurs in the DC port of converters. It can be seen in Fig. 3(a).

The diagram of the fault characteristic shown in Fig. 3(b) is obtained based on simulations. The detailed theoretical analysis of stages after short-circuit fault can be derived from [23] and [37]. According to the requirement of UPS, the fault should be cleared as fast as possible. Otherwise the drop of the DC bus voltage will cause the interruption of the load power. Thus, the stage before the DC bus voltage drops to 90% is analyzed. During this stage, the energy source module or storage module can be assumed as a constant-voltage source in order to simplify the analysis. The analytical fault model shown in Fig. 4 is used to analyze the characteristics of the fault current. It is assumed that the short-circuit fault occurs between the positive pole and negative pole in the DC port of Module N.



(a) Circuit model.



(b) The characteristic of fault current and bus voltage.

Fig. 3. Circuit model and the fault characteristic of Super-UPS.

Equation (1) is derived according to the simplified model in Fig. 4. The fault current in the DC port of modules can be derived by solving (1). For higher than third-order equations, numerical solutions are used to solve them.

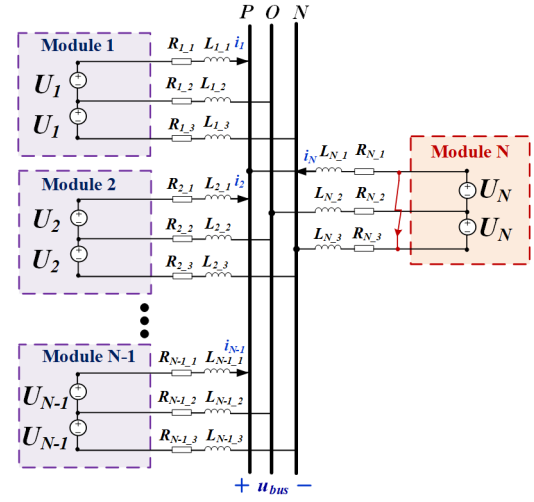


Fig. 4. Analytical model of the Super-UPS.

$$\begin{cases} (R_{1,1} + R_{1,3})i_1 + (L_{1,1} + L_{1,3})\frac{di_1}{dt} + u_{bus} = 2U_1 \\ (R_{2,1} + R_{2,3})i_2 + (L_{2,1} + L_{2,3})\frac{di_2}{dt} + u_{bus} = 2U_2 \\ \vdots \\ (R_{N-1,1} + R_{N-1,3})i_{N-1} + (L_{N-1,1} + L_{N-1,3})\frac{di_{N-1}}{dt} + u_{bus} = 2U_{N-1} \\ (R_{N,1} + R_{N,3})i_N + (L_{N,1} + L_{N,3})\frac{di_N}{dt} + u_{bus} = 0 \\ i_1 + \dots + i_{N-1} + i_N = 0 \end{cases} \quad (1)$$

where,  $L_{i,1}$ ,  $L_{i,2}$  and  $L_{i,3}$  are the line inductances.  $R_{i,1}$ ,  $R_{i,2}$  and  $R_{i,3}$  are the line resistances.  $U_i$  is the output voltages of module  $i$ ,  $i_i$  is the fault current of module  $i$ .  $u_{bus}$  is the voltage of common point in DC bus.

### C. Analysis of Fault Current Direction

Based on the fault model shown in Fig. 4, a typical case is used to analyze the characteristics of fault current when  $N$  equals three. The parameters of cables used for calculation are listed in TABLE V.

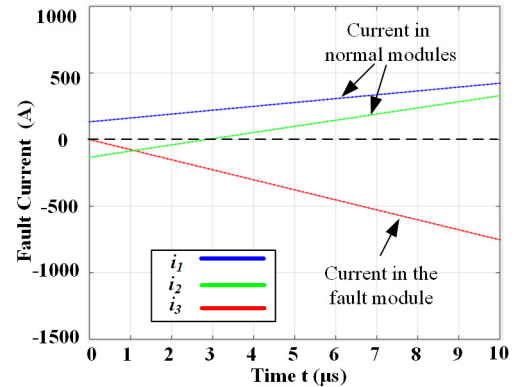


Fig. 5. Analytical results of the fault current.

The calculated result of fault current in the case is shown in Fig. 5. The initial condition is that Module 1 operates at the full load with a positive power flow. Module 2 is at the full load with a negative power flow. Module 3 is at no load. The power capacity of the modules is 100 kW, and DC bus voltage is 750 V. Then the rated current of the bus-side is 133 A. So, the initial



current of Module 1, 2 and 3 are 133 A, -133A and 0 A respectively. More detailed analysis of fault current is provided in [38].

It is found that the initial value of the current has a little impact on direction of fault current. Due to rapidly rising fault current, even though the initial direction of fault current ( $i_2$ ) in module 2 is negative, it becomes positive within a very short period (2.8  $\mu$ s). After that, the direction of fault current in the fault module is negative. The direction of fault current in all normal modules is positive. Besides, it can be proven that the derivative of the fault current in the fault module is always negative before the fault current reaches the minimum value, while the derivative of fault current in normal modules is positive. This characteristic of the fault current direction is the basis to design the protection scheme.

### III. FAST FAULT PROTECTION SCHEME WITHOUT COMMUNICATION

#### A. Proposed Protection Scheme

The concept of protection scheme for Super-UPS is shown in Fig. 6. The proposed scheme generates the decisions for breakers and converters based on local measurements. Firstly, the decisions for breakers depend on the directional current detection. According to the analysis of fault current characteristic, the fault current detection unit locates the fault based on the direction of fault current. Different thresholds for two directions are set to distinguish the module fault (F1) occurs. The threshold comparison for negative direction is used to trip the breaker when the module fault (F1) occurs. The threshold comparison for positive direction is used to trip the breaker when the bus-bar fault (F2) occurs. Secondly, the protection scheme coordinates with converters to ensure uninterruptible load power. It is based on the DC bus voltage detection and the directional current detection. The decisions for converters are generated by mode selection units. The converters change the modes according to the logic shown in Fig. 8. The protection scheme does not rely on any communication. A fast and robust protection is achieved, minimizing the fault affected area and ensuring uninterruptible load power.

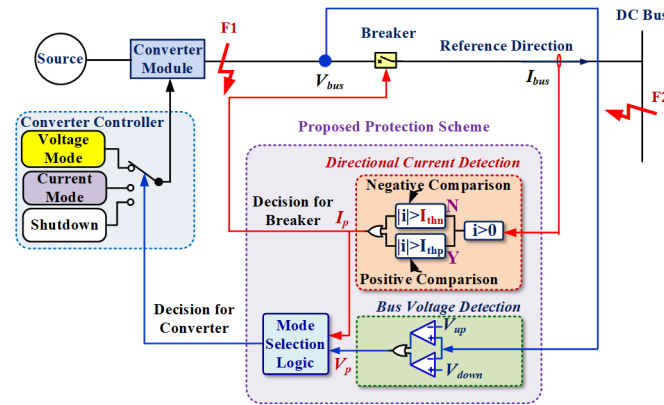


Fig. 6. Proposed protection scheme.

The coordination of breakers for different fault locations is shown in Fig. 7, and the decisions for breakers are given in TABLE II. In order to achieve the selective protection, the threshold for positive direction is higher than that for negative direction in the current detection unit. Taking the fault F1 as an

example, the fault current in S1 is negative, then S1 is tripped when current reaches the negative threshold  $I_{thn}$ , while the fault current in S2 is positive. Since the positive threshold  $I_{thp}$  is higher than  $I_{thn}$ , the S2 is not tripped. According to TABLE II, it can be seen that only the faulty part is isolated based on the direction of fault current. The fault-affected area is minimized.

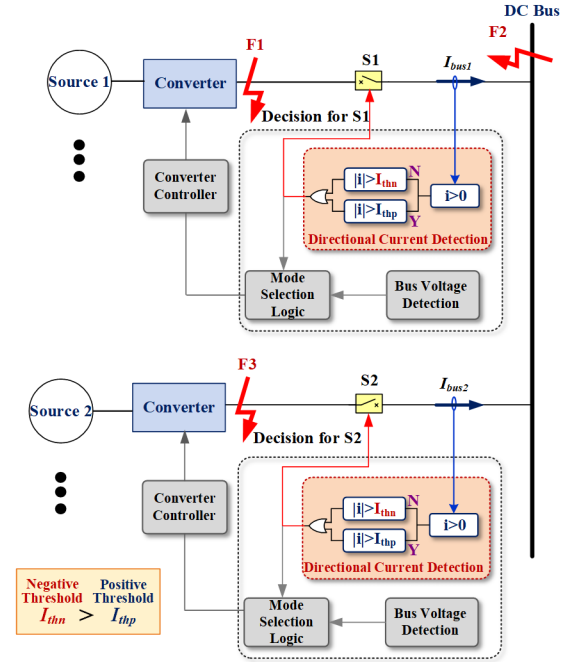


Fig. 7. The coordination of breakers for different fault locations.

TABLE II  
THE DECISIONS FOR BREAKERS

Fault Location	Fault Current Direction in S1	Fault Current Direction in S2	Decision for S1	Decision for S2
F1	Negative	Positive	Trip*	No trip
F2	Positive	Positive	Trip**	Trip**
F3	Positive	Negative	No trip	Trip

\*Negative threshold  $I_{thn}$  is reached, \*\* Positive threshold  $I_{thp}$  is reached

In order to achieve uninterruptible load power, it is necessary for the protection scheme to coordinate with converters in Super-UPS. The decision for converters is decided by the unit of mode selection logic in Fig. 6. It relies on the fault detection signal  $I_p$  and the bus voltage detection  $V_p$ . When DC bus voltage is lower than  $V_{down}$  or higher than  $V_{up}$ ,  $V_p$  turns to "1". When the fault is detected by directional current detection unit,  $I_p$  turns to "1". The detailed threshold setting rule is analyzed in Section III.B. The logic of mode selection is given in Fig. 8. The mode selection logic for the source module and the load module is different. For the source module, the converter changes its mode among voltage mode, current mode and shutdown. It should be noticed that the current-mode modules have priorities to change their modes to voltage mode when voltage-mode module fault occurs. For the load module, the load converter changes its mode between load mode and bypass mode. The coordination of protection is also based on local measurement without any message exchange with other modules.

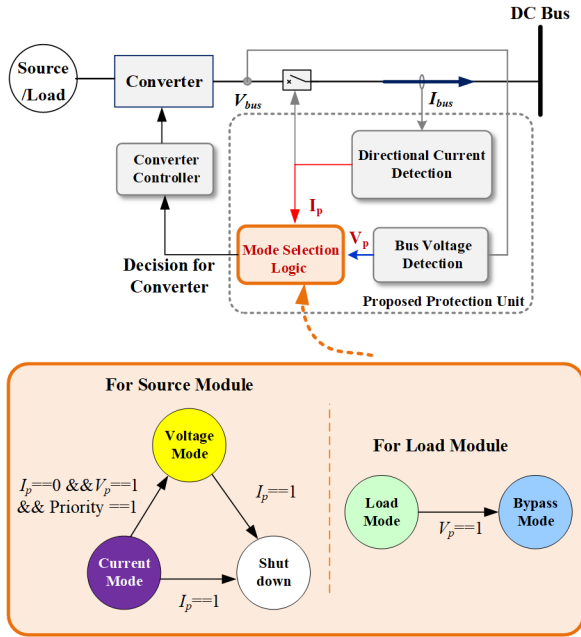


Fig. 8. The decision for converters in the protection scheme.

The Super UPS with proposed protection scheme is shown in Fig. 9. As a compact power supply, Super UPS is master-slave system. There is a bus voltage regulation converter (VRC) Module 1, a load inverter Module 2 and multiple current regulation converters (CRCs) Module 3~N. Module 3 is pre-configured as CRC #1, which has the highest priority as the backup module of VRC. The bypass switches are controlled by the load module.

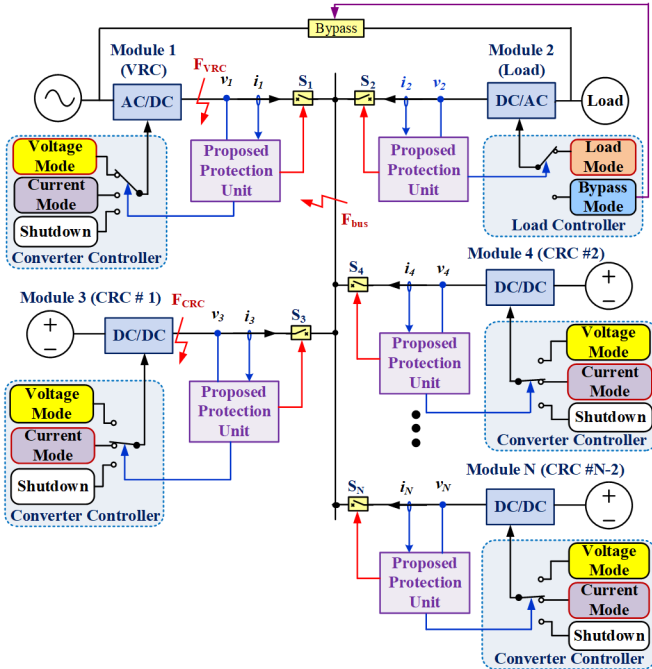
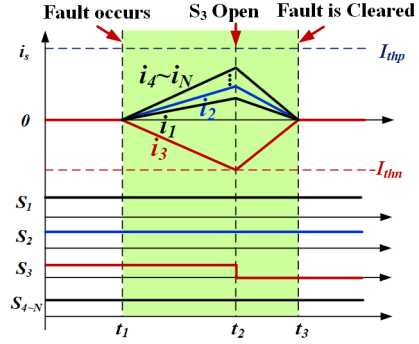


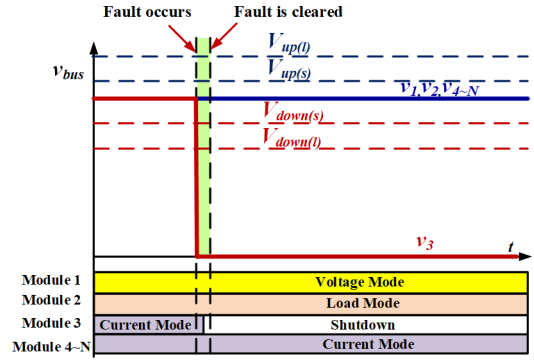
Fig. 9. Super UPS with the proposed protection method.

The operation of the protection scheme for different fault locations is analyzed from Fig. 10 to Fig. 12. The CRC fault  $F_{CRC}$ , VRC fault  $F_{VRC}$  and bus-bar fault  $F_{bus}$  are analyzed in detail. The decisions for breakers and converters under short-circuit fault  $F_{CRC}$  are shown in Fig. 10. In Fig. 10 (a), when the short-circuit fault occurs in Module 3 (CRC), the fault current in Module 3 is negative, while the fault current in other

modules is positive. Since the threshold for negative direction  $I_{thn}$  is set lower than threshold for positive direction  $I_{thp}$ , the  $S_3$  is tripped first. While, the SSCBs connected to other modules are not tripped. The selectivity of protection is achieved, and the area affected by the fault is minimized. After the Module 3 is isolated by SSCBs based on the direction of fault current, the controller of Module 3 shuts down the converter by the mode selection logic unit. The controllers of other modules do not need to change.



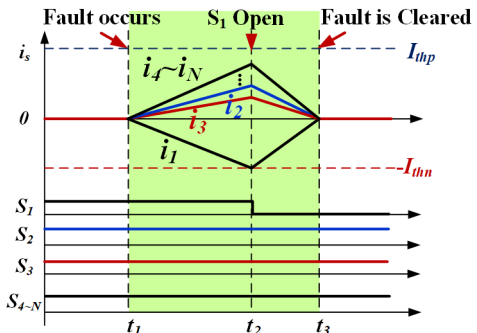
(a) Decisions for breakers.



(b) Decisions for converters.

Fig. 10. The operation of the protection when module CRC #1 fault occurs.

If short-circuit fault  $F_{VRC}$  occurs in Module 1 (VRC), then Module 1 is isolated by the SSCB based on directional current detection as shown in Fig. 11 (a). However, in this situation, the system loses the bus-voltage regulator VSC. The controller of the Module 3 (CRC #1) detects the DC bus voltage. When the bus voltage exceeds the bus voltage threshold of the source module  $V_{down(s)}$ , the controller of Module 3 changes its mode from the current control mode to the voltage control mode based on the mode selection logic. The Module 3 becomes the new VRC to regulate the bus voltage. The controllers of other modules do not need to change. The decisions for converters are shown in Fig. 11 (b).



(a) Decisions for breakers.





DC bus voltage of the load module drops to 90% of the rated bus voltage.

In order to avoid malfunctions, the reliability factors,  $K_{rel1}$  and  $K_{rel2}$ , can be introduced. Equation (2) can be rewritten as (3).

$$\begin{aligned} & \left[ \max \left\{ -3I_{r\_n}, |I_{dy}|, I_{sam\_down} \right\} \right] K_{rel1} < I_{thn} \\ & < \left[ \min \left\{ |I_{90\%}|, I_{cap\_max}, I_{pd\_max} \right\} - t_d \cdot k_{i\_max} \right] K_{rel2} \end{aligned} \quad (3)$$

### 2) Current threshold setting for positive direction

The threshold setting for positive direction has two functions. One is providing a backup protection when SSCBs installed in the fault module malfunction. The other one is tripping all SSCBs to isolate the DC bus-bar fault.

Compared with the threshold for negative direction, the positive threshold setting does not depend on the type of sources. Based on the requirement of coordination of SSCBs, the positive threshold of module  $i$  should be larger than the negative thresholds of all other modules. The range of positive threshold is given in (4).

$$\max \{ |I_{thn(1)}|, \dots, |I_{thn(i-1)}|, |I_{thn(i+1)}|, \dots, |I_{thn(N)}| \} < I_{thp(i)} \quad (4)$$

$(1 \leq i \leq N)$

where,  $I_{thp(i)}$  and  $I_{thn(i)}$  are the positive threshold and the negative threshold of module  $i$  respectively.

### 3) Voltage threshold setting for mode selection unit

The mode selection of the converter is based on the bus voltage detection. In Fig. 14, when the DC bus voltage is lower than  $V_{down}$  or higher than  $V_{up}$ , the mode selection unit is tripped to change the mode of converters based on the selection logic in Fig. 8. The ranges of  $V_{down}$  and  $V_{up}$  are given in (5) respectively.

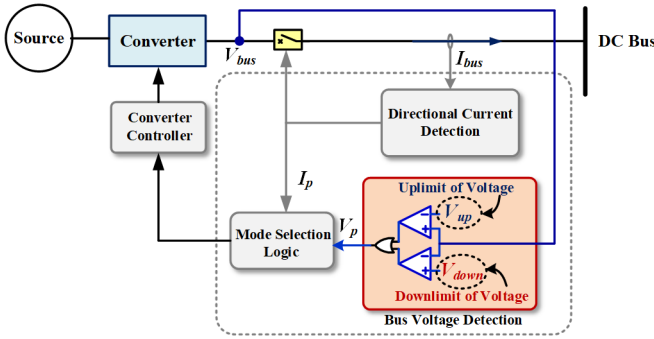


Fig. 14. Voltage threshold setting of protection scheme.

$$\begin{cases} \frac{2\sqrt{2}V_{load\_RMS}}{m_{inv}} < V_{down} < (1-p)V_r \\ (1+p)V_r < V_{up} < V_s \end{cases} \quad (5)$$

where,  $m_{inv}$  is the amplitude modulation ratio of the load inverter,  $V_{load\_rms}$  is the phase voltage of load inverter,  $p$  is the maximum fluctuation of bus voltage at the normal state,  $V_s$  is the maximum safe voltage for converters. As shown in (6), it should be noticed that the threshold voltage  $V_{down(l)}$  for the load module should be lower than the threshold  $V_{down(s)}$  for CRC. Otherwise, when VSC fault occurs in Fig. 11, the load module may change to bypass mode by mistake. Similarly,  $V_{up(l)}$  for load module should be higher than the threshold  $V_{up(s)}$  for CRC.

$$\begin{cases} V_{down(l)} < V_{down(s)} \\ V_{up(l)} > V_{up(s)} \end{cases} \quad (6)$$

### C. An Improved Fault Current Measurement Method for Accurate Operation of Protection Scheme

Due to the requirement of fast isolation, SSCBs need to be installed in the DC port of modules in the Super UPS. The realization of the proposed protection scheme with SSCBs is shown in Fig. 15. The directional fault current detection can be easily implemented into SSCB by setting collector-emitter voltage thresholds for the positive and negative switch respectively. However, there is a large measurement error for the traditional current measurement method based on the voltage drop of SSCB when the derivative of the fault current is high.

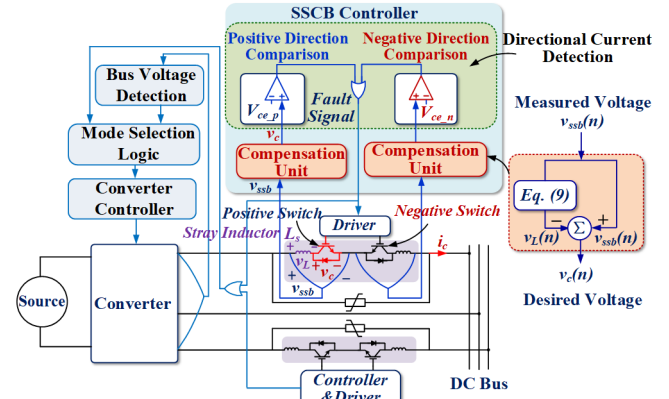


Fig. 15. Improved current measurement method for proposed protection scheme.

Because of the existence of stray inductor  $L_s$  in the Insulated Gate Bipolar Transistor (IGBT) module in Fig. 15, the measured  $v_{ssb}$  voltage consists of the desired IGBT chip voltage  $v_c$  and stray inductor voltage drop  $v_L$ . The stray inductor voltage is directly proportional to the derivative of current. For the same value of current with different derivatives, the measured voltage of SSCB is quite different. In Fig. 16, assuming that the current derivative is 30 A/μs which is a typical value in Super-UPS and the stray inductance is 20 nH, the threshold for steady current is 300 A. The same threshold will be reached when current is 50 A with derivative of 30 A/μs.

An improved measurement method is proposed to eliminate the effect of stray inductor on the measurement. In the proposed method, the voltage drop of SSCB is sampled by the digital controller, and the extra voltage caused by stray inductor is eliminated by the compensation unit shown in Fig. 15. The compensated results are sent to a comparison unit to trip the breaker. The compensation unit is based on the linear zone of IGBT output characteristic curve, which is shown as Zone II of Curve 1 in Fig. 16.  $I_{min}$  is defined as the minimum current of Zone II. When the current is larger than  $I_{min}$ , the relationship between voltage  $V_{ce}$  and current  $I_c$  of IGBT is linear. It can be expressed as (7).

$$V_{ce}(I_c) = kI_c + b \quad (I_c \geq I_{min}) \quad (7)$$

where,  $k$  and  $b$  are the fitting coefficients of IGBT output characteristic curve.

According to Fig. 15 and (7), (8) is derived with the assumption of the constant current derivative during the short analyzed period.

$$\begin{cases} v_L(t) = \frac{L_s}{k} \frac{dv_{ssb}(t)}{dt} \\ v_c(t) = v_{ssb}(t) - \frac{L_s}{k} \frac{dv_{ssb}(t)}{dt} \end{cases} \quad (8)$$

where,  $L_s$  is stray inductance of SSCB,  $k$  is the parameter in (7).

According to (8), the voltage drop of the stray inductors  $V_L$  and desired IGBT chip voltage  $V_c$  is related to the derivative of the measured voltage drop of SSCB  $V_{ssb}$ . Since, the derivative calculation is sensitive to the sampling error, a least-square (LS) method is applied in order to reduce the measurement error. In the LS method, adjacent three points are used to calculate the derivative, which is shown in Fig. 17. After discretizing (8), the voltage-drop of the stray inductors  $V_L$  can be expressed in (9), and the desired  $V_c$  voltage is shown in (10).  $T_s$  is the sampling period.

$$v_L(n) = L_s \frac{v_{ssb}(n) - v_{ssb}(n-2)}{2kT_s} \quad (9)$$

$$v_c(n) = v_{ssb}(n) - v_L(n) = (1 - \frac{L_s}{2kT_s})v_{ssb}(n) + \frac{L_s}{2kT_s}v_{ssb}(n-2) \quad (10)$$

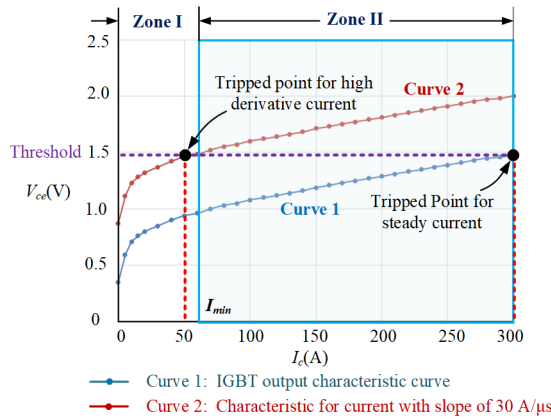


Fig. 16. The effect of stray inductor on the current measurement.

In (10), it can be seen that the calculation result of  $V_c$  only depends on voltage drop of SSCB, sampling period and inductance of stray inductor. It does not use the information of current. The calculated result  $V_c$  is compared with the threshold to trip the SSCB. According to the IGBT output characteristic curve in Fig. 16, the threshold of  $V_c$  can be derived by the desired fault current threshold. The threshold  $I_{thn}$  and  $I_{thp}$  shown in Fig. 13 can be converted to the  $V_{ce\_n}$  and  $V_{ce\_p}$  of SSCB using (7). The  $V_{ce\_n}$  and  $V_{ce\_p}$  are derived as given in (11).

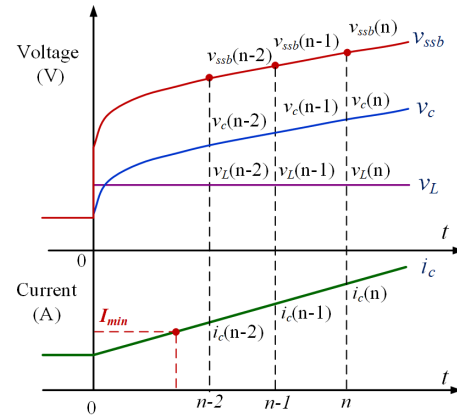


Fig. 17. The calculation of stray inductor voltage for the improved measurement method.

$$\begin{cases} V_{ce\_n} = kI_{thn} + b \\ V_{ce\_p} = kI_{thp} + b \end{cases} \quad (11)$$

It should be noticed that the current at the first valid point used for calculation should be larger than  $I_{min}$ . Thus, the protection threshold settings should meet the requirement of (12). Otherwise, the calculated results used for tripping the SSCB will be invalid.

$$I_{thn/thp} \geq I_{min} + 2T_s k_f \quad (12)$$

where,  $k_f$  is the derivative of fault current.

#### D. Comparison between Proposed Protection Method and Conventional Methods

A comparison between the proposed method and other methods is provided in TABLE III. The fault clearing time for different types of faults and the reliability of load power are compared. The data of the proposed method is based on the experimental results. For the directional overcurrent protection method [35], the fault detection only responses for one direction of fault current. The breakers are tripped only for the module fault. It does not operate for bus-bar fault. Besides, the load is interrupted when the fault occurs in the common bus. The handshaking method [9] does not rely on communication, and it improves the robustness of protection. However, all converters are shut down after the fault is detected. The loads on the healthy buses are interrupted temporarily. For the directional comparison protection [23] and hybrid protection method [17], [33], the protection speed may not meet the requirement of protection in the compact power supply due to

TABLE III  
COMPARISON BETWEEN THE PROPOSED METHOD AND OTHER METHODS

Methods	Clearing Time for Module Faults	Clearing Time for Bus Faults	Assistance of Communication	Uninterruptible Load Power	System Topology
Directional overcurrent protection method in [35]	3 ms	Unhandled	No	No	Radial
Directional comparison protection method in [23]	Not mentioned	2 ms	Yes	Yes*	Meshed
Handshaking method in [9]	Not mentioned	500 ms	No	Temporary Interruption	Meshed
Combination of differential and overcurrent protection in [33]	5 ms	1 ms	Yes	Yes*	Meshed
Hybrid protection method in [17]	70 μs	100 μs	Yes	No	Radial
Proposed protection method	13 μs	22 μs	No	Yes	Radial

\* For the compact power supply system, it may cause temporary interruption of load due to the communication delay.

the dependence on communication. It will cause the interruption of load power.

The proposed scheme has three metrics for the compact and uninterruptible power supply system: (1) Detecting both module faults and bus-bar faults locally and quickly, (2) Ensuring the uninterruptible load power without assistance of communication, (3) Accurate and reliable operation of protection for rapidly rising fault current by the improved measurement method. Thus, the protection speed and the reliability of load are improved.

#### IV. EXPERIMENTAL RESULTS

##### A. Prototype of Super-UPS

The prototype of a Super-UPS is built to verify the proposed protection scheme. In the prototype, there are two kinds of standard converter modules, bi-directional AC/DC module and bi-directional DC/DC module. The SSCBs are installed in the DC bus-side of the converter modules. The metal oxide varistors (MOVs) are used to protect the SSCBs. The prototype of the Super-UPS is shown in Fig. 18. The parameters of the standard converter modules and SSCBs are shown in TABLE IV. The architecture of the system is shown in Fig. 19. The line parameters among modules are given in TABLE V.

TABLE IV

THE SPECIFICATIONS OF THE MODULES IN SUPER UPS

Standard Bi-directional AC/DC		Standard Bi-directional DC/DC	
Item	Value	Item	Value
Power capacity	100 kW	Power capacity	30 kW
Input voltage	380 V	Input range	200-400 V
Input inductor	0.38 mH	Input inductor	0.32 mH
Input capacitor	200 $\mu$ F	Input capacitor	400 $\mu$ F
Output capacitor	4400 $\mu$ F	Output capacitor	400 $\mu$ F
Rated bus-side voltage	$\pm 375$ V	Rated bus-side voltage	$\pm 375$ V
Rated current in bus-side	133 A	Rated current in bus-side	40 A

SSCB			
IGBT model number	FF450R12KE4_E	MOV model number	EPCOS
IGBT rated voltage	1200 V	MOV varistor voltage	470 V
IGBT rated current	450 A		

TABLE V

THE CABLE PARAMETERS OF VERIFICATION

Module 1		Module 2	
Module type	Standard AC/DC	Module type	Standard AC/DC
Line inductor $L_{1,1}$	3.8 $\mu$ H	Line inductor $L_{2,1}$	2.2 $\mu$ H
Line inductor $L_{1,2}$	1.8 $\mu$ H	Line inductor $L_{2,2}$	1.3 $\mu$ H
Line inductor $L_{1,3}$	3.2 $\mu$ H	Line inductor $L_{2,3}$	2.2 $\mu$ H
Line resistor $R_{1,1}$	4.8 m $\Omega$	Line resistor $R_{2,1}$	2.8 m $\Omega$
Line resistor $R_{1,2}$	2.5 m $\Omega$	Line resistor $R_{2,2}$	1.6 m $\Omega$
Line resistor $R_{1,3}$	4.4 m $\Omega$	Line resistor $R_{2,3}$	2.8 m $\Omega$

Module 3			
Module type	Standard DC/DC	Line resistor $R_{3,1}$	6.5 m $\Omega$
Line inductor $L_{3,1}$	5.0 $\mu$ H	Line resistor $R_{3,2}$	1.7 m $\Omega$
Line inductor $L_{3,2}$	1.3 $\mu$ H	Line resistor $R_{3,3}$	2.9 m $\Omega$
Line inductor $L_{3,3}$	2.2 $\mu$ H		

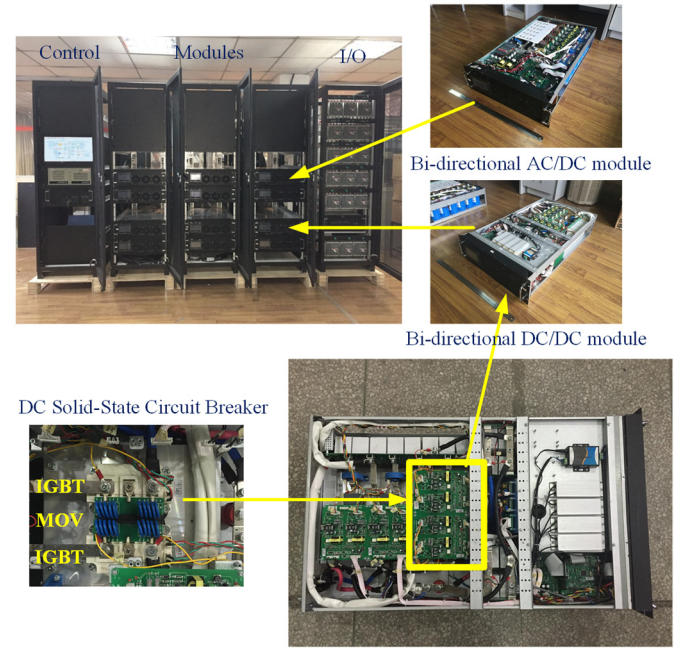
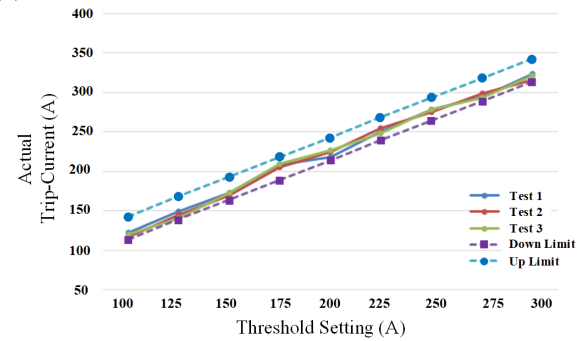


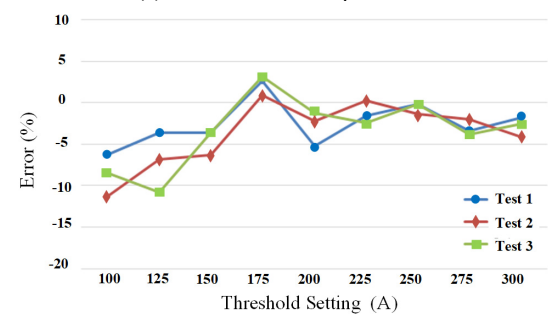
Fig. 18. Prototype of Super-UPS and SSCBs.

##### B. Accuracy Test of Fault Current Threshold Setting

The accuracy test of the proposed measurement method with stray inductor voltage compensation is shown in Fig. 20. The sampling frequency of digital controller is 1 MHz. The theoretical down-limit and up-limit are calculated based on the time delay of digital processing and marked in Fig. 20 (a). It can be seen that the three test results are within the theoretical limits. The error between the trip-current and threshold is shown in Fig. 20 (b).



(a) Absolute value of trip-current.



(b) Error of the trip-current.

Fig. 20. Three test results of trip-current of SSCB (@ current derivative 29 A/ $\mu$ s).



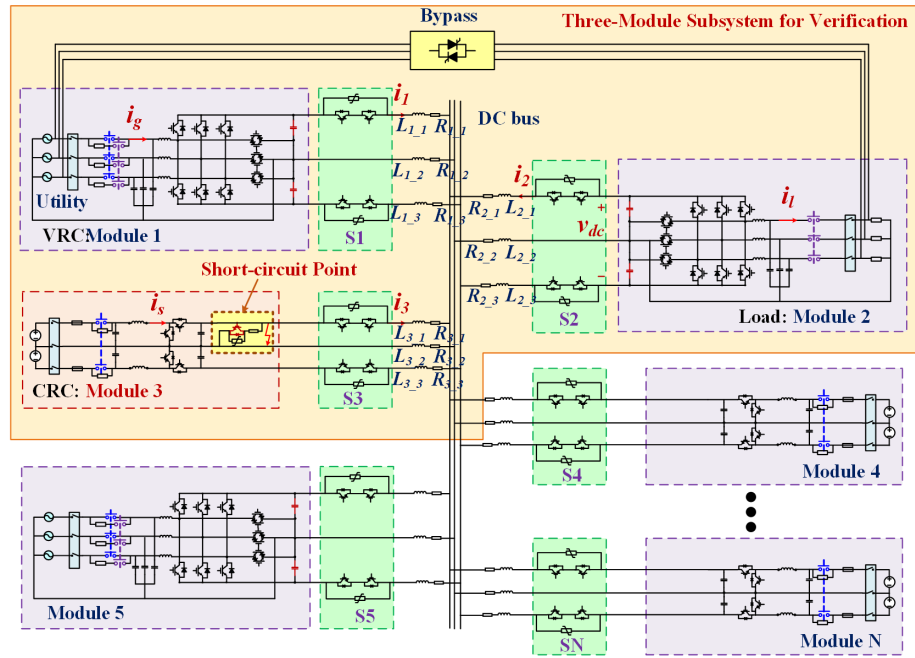


Fig. 19. The architecture of Super-UPS.

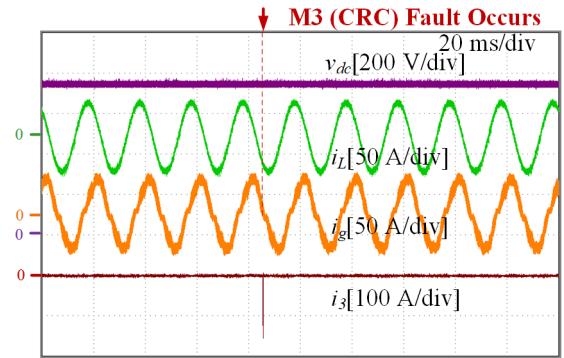
### C. Verification of Protection Scheme

The Super-UPS is designed modularly and configured flexibly. In Fig. 19, three modules are configured to verify the protection scheme of the system. Module 1 (M1) regulates the bus voltage. Module 2 (M2) is the load. Module 3 (M3) controls the output power. The bypass is installed to connect the utility and load. A 1700V/2400A IGBT is used to simulate the short-circuit fault point. MOV is also used to protect the IGBT at the short-circuit point. The threshold setting of the module is given in Appendix. A.

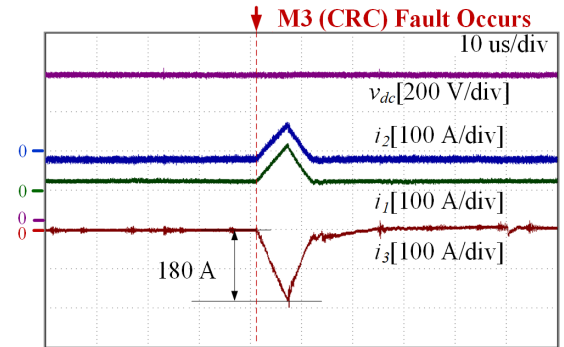
The protections for different fault locations are verified. The fault locations include CRC, VRC, and the DC bus-bar. Firstly, the fault occurs in the bus-side of CRC M3. The protections under different operation points are tested. In the test, the rated power of load is 30 kW. In Fig. 21, the initial power of M1, M2 and M3 are 20 kW, -20 kW and 0 kW respectively. From Fig. 21 (a), it can be seen that there is no change of load current and input current of normal module when short-circuit fault occurs. The DC bus voltage of load M2 is also kept constant. During the fault, the load is not interrupted. In Fig. 21 (b), the characteristic of fault current direction is shown clearly. The fault current flows through the SSCB S3 connected to fault module M3 is negative. The fault current in normal modules M1 and M2 increase positively. The direction of fault current is used to locate the fault module. The threshold for negative direction is set to be 120 A. Because of the time delay in the protection, the final turn-off fault current of the SSCB in module 3 is -180 A. During the fault, there is no dip of the DC bus voltage of M2. The fault is cleared within 11  $\mu$ s.

The protection waveforms under another initial state is shown in Fig. 22. The initial power of M1, M2 and M3 are 0 kW, -20 kW and 20 kW respectively. Before the fault occurs, M1 regulates the DC bus voltage and M3 provides the load power. It can be seen that M3 is isolated after the fault. M1 provides the load power. In Fig. 22 (b), the turn-off fault current

in fault module is -178 A. The fault is cleared within 13  $\mu$ s. It also shows that the load is not interrupted in this situation.



(a) Overall protection waveforms.

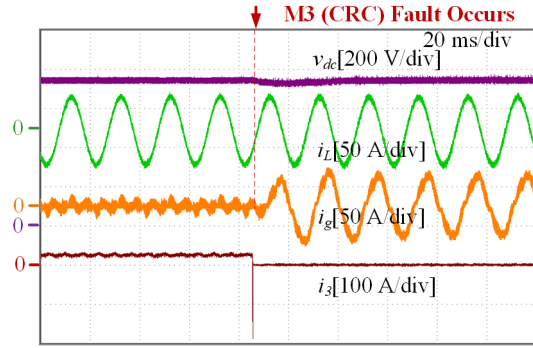


(b) Detailed waveforms at the fault time.

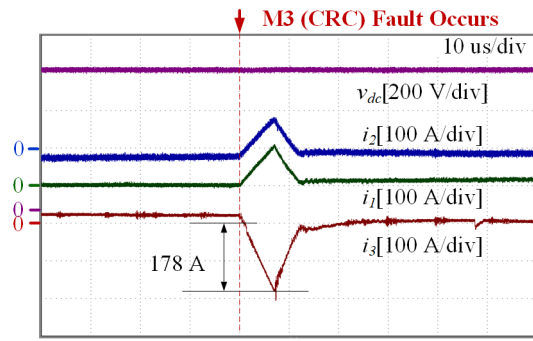
Fig. 21. The protection waveforms when a fault occurs in CRC M3 (M1: 20 kW, M2: -20 kW, M3: 0 kW).

Next, the fault location is in the bus-side of VRC M1. When the fault occurs in M1, the waveforms of protection is shown in Fig. 23. M1 is isolated by the SSCB when the fault current reaches the negative threshold. The system loses VRC, and the DC bus voltage begins to decrease after M1 is isolated. M3 detects the DC bus voltage, and its operation mode change from current control mode to bus voltage control mode when the bus

voltage drops to the threshold of 720 V. It can be seen that the load is not interrupted during the transferring. The initial current direction of modules and the fault condition in Fig. 24 are the same as Fig. 23, however, the load level is half. Similarly, the load is not interrupted during the fault.

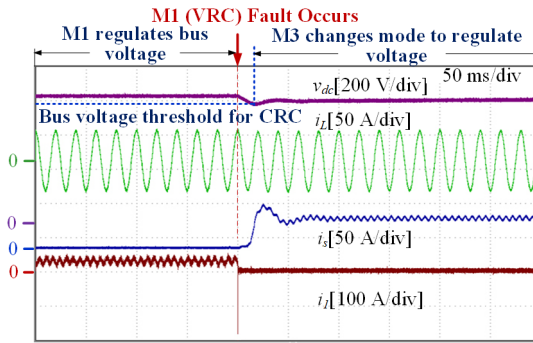


(a) Overall protection waveforms.

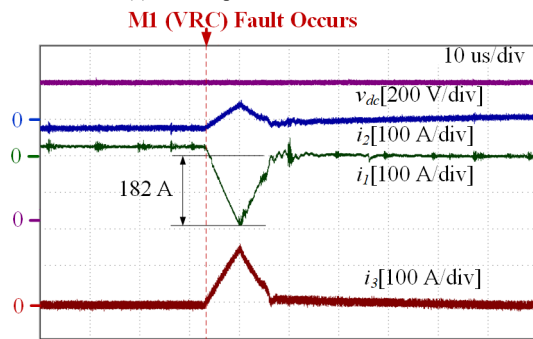


(b) Detailed waveforms at the fault time.

Fig. 22. The protection waveforms when a fault occurs in CRC M3 (M1: 0 kW, M2: -20 kW, M3: 20 kW).

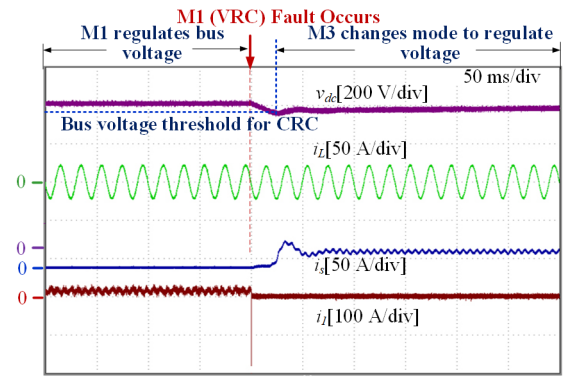


(a) Overall protection waveforms.

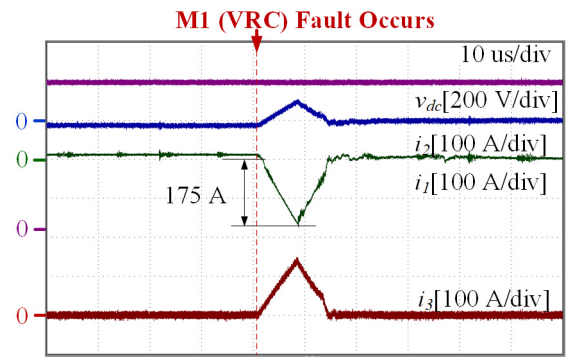


(b) Detailed waveforms at the fault time.

Fig. 23. The protection waveforms when a fault occurs in VRC M1 (M1: 20 kW, M2: -20 kW, M3: 0 kW).

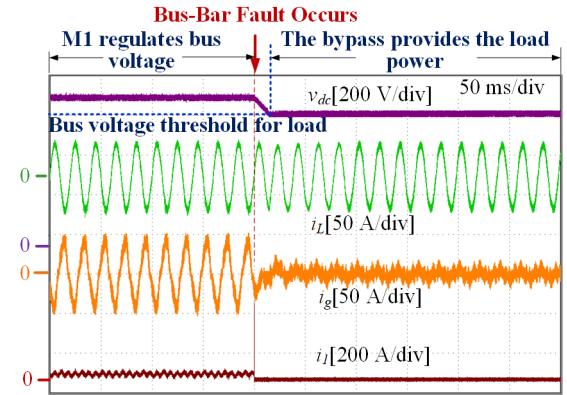


(a) Overall protection waveforms.

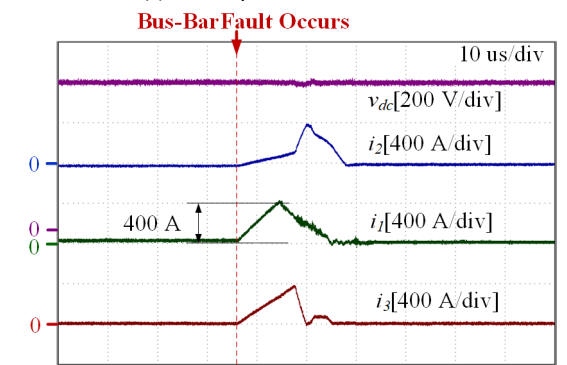


(b) Detailed waveforms at the fault time.

Fig. 24. The protection waveforms when a fault occurs in VRC M1 (M1: 10 kW, M2: -10 kW, M3: 0 kW).



(a) Overall protection waveforms.



(b) Detailed waveforms at the fault time.

Fig. 25. The protection waveforms when a fault occurs in DC bus-bar (M1: 20 kW, M2: -20 kW, M3: 0 kW).

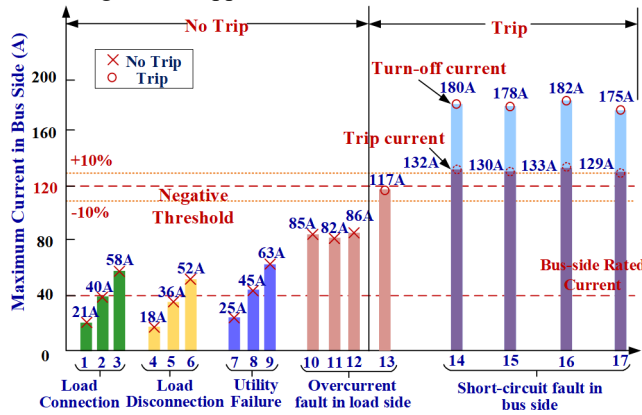
Thirdly, the fault location is in the DC bus-bar. When the fault occurs in the DC bus, all SSCBs are tripped and all modules are isolated. The fault is cleared within 22  $\mu$ s. The load inverter detects the DC bus voltage and turn on the bypass



switches when bus voltage drops to the threshold of 700 V. The bypass provides the load power after the fault is isolated. From Fig. 25 (a), it can be seen that the load is not interrupted when the fault occurs in the DC bus.

#### D. Sensitivity Discussion of Protection Scheme

Based on the experimental scheme shown in Fig. 19, the sensitivity of protection scheme under different conditions is tested, and the experimental results are shown in Fig. 26. Multiple operation conditions including load connecting, load disconnecting, overcurrent fault in load side and utility failure at different load levels are considered. In Fig. 26, it shows that there is no false tripping of protection for the conditions of load connecting, load disconnecting and utility failure. For the overcurrent fault in load side, there is no false tripping when the overcurrent threshold of load side is 1.5 times of the rated load current. However, if the overcurrent threshold of load side is larger than twice of the rated load current, the false tripping of bus-side SSCBs occurs. If there is special need for the system to operate at more than twice of rated load current, the threshold of protection scheme needs to be redesigned. For the short-circuit faults in bus side, Fig. 26 shows that the protection is tripped accurately. The difference between the trip current and the turn-off current is caused by the protection delay and high derivative of fault current. In addition, the fault current is large enough to trip the threshold when the short-circuit fault occurs in bus side. The influence of line impedance on fault current is given in Appendix. B.



(a) The results of sensitivity tests.

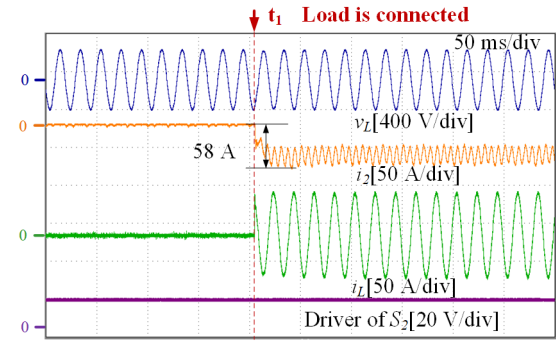
Condition	Index	Description
Load Connection	1	1/3 Load
	2	2/3 Load
	3	Full Load
Load Disconnection	4	1/3 Load
	5	2/3 Load
	6	Full Load
Utility Failure	7	1/3 Load
	8	2/3 Load
	9	Full Load
Overcurrent fault in load side	10	1/3 Load, Overcurrent threshold: $1.5 \times I_r^*$
	11	2/3 Load, Overcurrent threshold: $1.5 \times I_r$
	12	Full Load, Overcurrent threshold: $1.5 \times I_r$
	13	Full Load, Overcurrent threshold: $2 \times I_r$
Short-circuit fault in bus side	14	CRC Fault 1 (Fig. 21)
	15	CRC Fault 2 (Fig. 22)
	16	VRC Fault 1 (Fig. 23)
	17	VRC Fault 2 (Fig. 24)

\* $I_r$ : rated load current

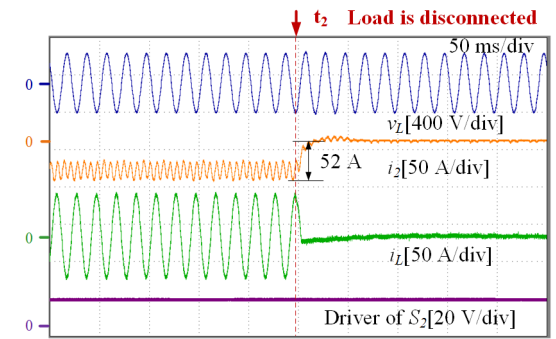
(b) Description of the cases.

Fig. 26. Experiment results for sensitivity analysis.

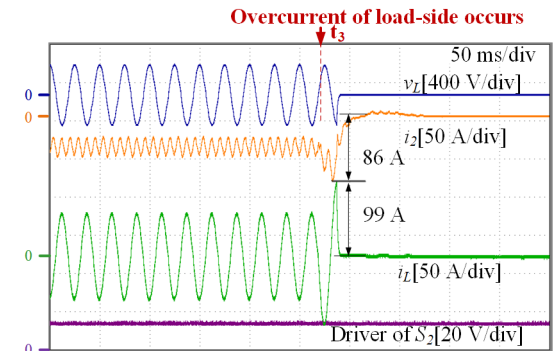
The experimental results at full load are shown in Fig. 27. In Fig. 27 (a), the breaker of load side is closed at  $t_1$ , and the 30 kW load is connected. The maximum transit current flowing through the SSCB S2 in bus side is 58 A, which is lower than the threshold 120 A. In Fig. 27 (b), the load is disconnected at  $t_2$ . Fig. 27 (c) shows the waveform under the condition of overcurrent fault in load side. Before the fault, the load power is 30 kW. The overcurrent fault of load side occurs at  $t_3$ , and the load current increases dramatically to the overload threshold of load side (1.5 times of the rated load current). The sensitivity under utility failure is tested in Fig. 27 (d). The utility fails at  $t_4$ , and M1 shuts down while M3 begins to provide the power of load. There is no false tripping of SSCBs under these conditions. In addition, the false tripping of protection at overcurrent fault of load side (twice of the rated load current) is shown in Fig. 28. The SSCB in bus side is tripped when the current reaches the negative threshold. Thus, for the protection design of Super UPS, the overcurrent threshold of load side should be less than twice of the rated load current.



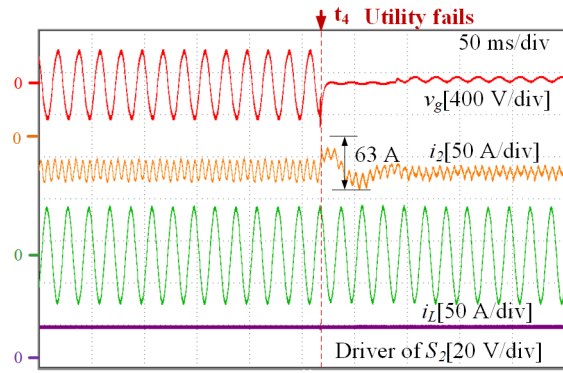
(a) The sensitivity of load connecting.



(b) The sensitivity of load disconnecting.



(c) The sensitivity of overcurrent fault in load side.



(d) The sensitivity of utility failure.

Fig. 27. The sensitivity of protection scheme under different conditions.

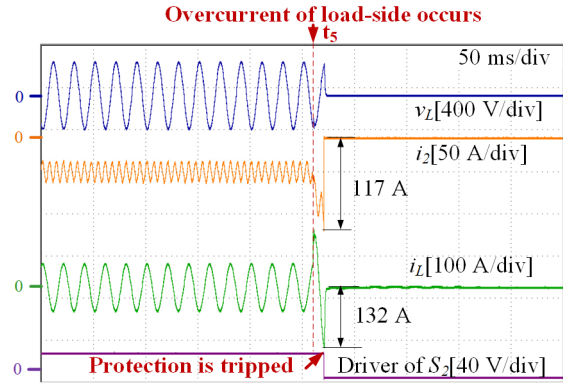


Fig. 28. The false tripping of protection at overcurrent fault (2x rated current) in load side.

## V. CONCLUSION

In this paper, a fast protection scheme based on the fault current direction is proposed for a Super-UPS which is a compact and high-surety power supply system. The scheme achieves fast fault detection and location based on direction of current. The protection strategy coordinated with converters, which is based on the fault current detection and DC bus voltage detection, is investigated to achieve the uninterruptable load power. The rules of threshold setting are introduced for reliable operation of protection. Different thresholds for two directions are set to distinguish the module fault and bus-bar fault. The protection scheme does not rely on any communication, so a high-speed and a high-reliable protection is achieved. Besides, an improved fault current measurement, which reduces the current measurement error caused by the stray inductor of SSCB, is proposed to guarantee an accurate operation of protection for rapidly rising fault current. Finally, the proposed protection strategy and improved current measurement are verified on the platform of the Super-UPS. The proposed protection scheme can be applied in systems which have similar characteristics with Super-UPS, such as electric-vehicle (EV) charging stations with integrated photovoltaic (PV) and battery energy storage, DC UPS for IDC etc. However, if the proposed scheme is applied to general DC microgrids, distribution line faults, other topologies and operation conditions should be considered, and further studies are needed.

## APPENDIX

### A. The Threshold Setting for Modules in Super-UPS

Take the bi-directional DC/DC module in Super-UPS as an example, the parameters used for the threshold calculation is shown in TABLE VI.

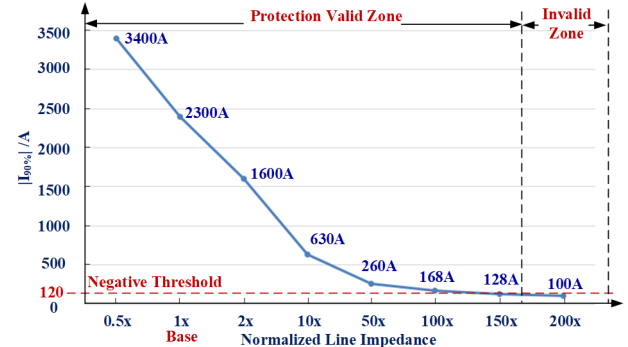
TABLE VI  
PARAMETERS USED FOR THRESHOLD CALCULATION

Item	Value	Item	Value
Negative Rated Current ( $I_{r,n}$ )	-40 A	DC Bus Capacitor ( $C_{bus}$ )	400 $\mu$ F
Down-limit of Sampling Method ( $I_{sam\_down}$ )	120 A	$I_{90\%}$	-2.3 kA
The Maximum Transient Current ( $I_{dt}$ )	-51 A	Maximum Protection delay ( $t_d$ )	2.7 $\mu$ s
Maximum Current ( $I_{pd\_max}$ ) of IGBT in SSCB	1.3 kA	Maximum di/dt ( $k_{i\_max}$ )	30 A/ $\mu$ s
Maximum Current ( $I_{cap\_max}$ ) of DC Capacitors	8 kA	Reliability Factor ( $K_{rel1}$ , $K_{rel2}$ )	1

According to (3), the threshold for negative direction is set to be 120 A. The threshold for the positive direction is 360 A. Besides, the down-limit of bus voltage  $V_{down}$  for the source module is set to be 720 V. The up-limit  $V_{up}$  is 780 V based on (5).

### B. The Influence of Line Impedance on Protection Scheme

According to (3), in order to avoid malfunctions of protection, the negative threshold should be less than  $I_{90\%}$  which is the fault current value when the DC bus voltage drops to 90% of the rated bus voltage. Based on simulations, Fig. 29 shows the relationship between the  $I_{90\%}$  and normalized line impedance for CRC fault in Fig. 19. The values of line parameters given in TABLE V are regarded as the base values ("1x"). For example, "10x" means that each line parameter in Fig. 19 equals ten times of the value given in TABLE V. It can be seen that  $I_{90\%}$  is not large enough to trip the threshold only when the line impedance is larger than 200 times of the base value. However, in this situation, the maximum line inductance among modules reaches 1.76 mH, and the line distance is approximately 3.8 km which is too long for the compact power supplies and UPSs. Thus, for compact power supplies, the fault current is large enough to trip the threshold when the short-circuit fault occurs.

Fig. 29. Relationship between normalized line impedance and  $I_{90\%}$ .

## REFERENCES

- [1] D. Xu, H. Li, Y. Zhu, K. Shi, and C. Hu, "High-surety Microgrid: Super Uninterruptable Power Supply with Multiple Renewable Energy Sources",

- Electric Power Components and Systems*, vol. 43, no. 8-10, pp. 839-853, Jun. 15, 2015
- [2] "IEEE recommend practice for 1 kV to 35 kV Medium-Voltage DC Power System on Ship", *IEEE Standard 1709*, 2010.
  - [3] F. Liu, W. Liu, X. Zha, H. Yang, and K. Feng, "Solid-State Circuit Breaker Snubber Design for Transient Overvoltage Suppression at Bus Fault Interruption in Low-Voltage DC Microgrid," *IEEE Transactions on Power Electronics*, vol. 32, no. 4, pp. 3007-3021, April 2017.
  - [4] C. Meyer, and R.W. De Doncker, "Solid-State Circuit Breaker Based on Active Thyristor Topologies," *IEEE Transactions on Power Electronics*, vol.21, no.2, pp.450-458, Mar. 2006.
  - [5] R. Schmerda, R. Cuzner, R. Clark, D. Nowak, and S. Bunzel, "Shipboard Solid-State Protection: Overview and Applications," *IEEE Electrification Magazine*, vol. 1, no. 1, pp. 32-39, Sep. 2013.
  - [6] Z. J. Shen, G. Sabui, Z. Miao and Z. Shuai, "Wide-Bandgap Solid-State Circuit Breakers for DC Power Systems: Device and Circuit Considerations," *IEEE Transactions on Electron Devices*, vol. 62, no. 2, pp. 294-300, Feb. 2015.
  - [7] Solid-State DC Circuit Breaker, by Q. Huang, X. Zhou and Z. Xu, (2003, Oct. 2) *Patent US 2003/0183838 A1*.
  - [8] R. M. Cuzner and G. Venkataramanan, "The Status of DC Micro-Grid Protection," in *Proc. IEEE Industry Applications Society Annual Meeting 2008*, pp. 1-8, Oct. 2008.
  - [9] L. Tang, and B.-T. Ooi, "Locating and Isolating DC Faults in Multi-Terminal DC Systems," *IEEE Transactions on Power Delivery*, vol.22, no.3, pp.1877-1884, Jul. 2007.
  - [10] P. Cairoli and R. A. Dougal, "Fault Detection and Isolation in Medium-Voltage DC Microgrids: Coordination Between Supply Power Converters and Bus Contactors," *IEEE Transactions on Power Electronics*, vol. 33, no. 5, pp. 4535-4546, May 2018.
  - [11] M. Monadi, C. Gavriluta, A. Luna, J. I. Candela and P. Rodriguez, "Centralized Protection Strategy for Medium Voltage DC Microgrids," *IEEE Transactions on Power Delivery*, vol. 32, no. 1, pp. 430-440, Feb. 2017.
  - [12] M. Farhadi, and O. A. Mohammed, "A New Protection Scheme for Multi-Bus DC Power Systems Using an Event Classification Approach", *IEEE Transactions on Industry Applications*, vol. 52, no. 4, pp. 2834-2842, July-Aug. 2016
  - [13] J. D. Park, J. Candelaria, L. Ma, and K. Dunn, "DC Ring-Bus Microgrid Fault Protection and Identification of Fault Location", *IEEE Transactions on Power Delivery*, vol. 28, no. 4, pp. 2574-2584, Oct. 2013.
  - [14] E. Sortomme, S. S. Venkata, and J. Mitra, "Microgrid Protection Using Communication-Assisted Digital Relays", *IEEE Transactions on Power Delivery*, vol. 25, no. 4, pp. 2789-2796, Oct. 2010.
  - [15] A. Maqsood, and K. Corzine, "DC Microgrid Protection: Using the Coupled-Inductor Solid-State Circuit Breaker," *IEEE Electrification Magazine*, vol. 4, no. 2, pp. 58-64, June 2016.
  - [16] S. D. A. Fletcher, P. J. Norman, S. J. Galloway, and G.M. Burt, "Determination of Protection System Requirements for DC Unmanned Aerial Vehicle Electrical Power Networks for Enhanced Capability and Survivability," *IET Electrical Systems in Transportation*, vol.1, no.4, pp.137-147, Dec. 2011.
  - [17] A. A. S. Emhemed, K. Fong, S. Fletcher, and G. M. Burt, "Validation of Fast and Selective Protection Scheme for an LVDC Distribution Network," *IEEE Transactions on Power Delivery*, vol. 32, no. 3, pp. 1432-1440, June 2017.
  - [18] M. E. Baran, and N. R. Mahajan, "Overcurrent Protection on Voltage-Source-Converter-Based Multiterminal DC Distribution Systems," *IEEE Transactions on Power Delivery*, vol.22, no.1, pp.406-412, Jan. 2007.
  - [19] M. Fang, L. Fu, R. Wang, and Z. Ye, "Coordination protection for DC distribution network in DC zonal shipboard power system," in *Proc. International Conference on Advanced Power System Automation and Protection (APAP) 2011*, vol.1, pp.418-421, Oct. 2011.
  - [20] D. Salomonsson, L. Soder, and A. Sannino, "Protection of Low-Voltage DC Microgrids," *IEEE Transactions on Power Delivery*, vol.24, no.3, pp.1045-1053, Jul. 2009.
  - [21] E. Cinieri, A. Fumi, V. Salvatori, and C. Spalvieri, "A New High-Speed Digital Relay Protection of the 3-kVdc Electric Railway Lines," *IEEE Transactions on Power Delivery*, vol. 22, no. 4, pp. 2262-2270, Oct. 2007.
  - [22] E. Christopher, M. Sumner, D. W. P. Thomas, X. Wang, and F. de Wildt, "Fault Location in a Zonal DC Marine Power System Using Active Impedance Estimation," *IEEE Transactions on Industry Applications*, vol. 49, no. 2, pp. 860-865, March-April 2013.
  - [23] R. Mohanty, and A. K. Pradhan, "Protection of Smart DC Microgrid with Ring Configuration using Parameter Estimation Approach," *IEEE Transactions on Smart Grid*, to be published.
  - [24] S. D. A. Fletcher, P. J. Norman, S. J. Galloway, P. Crolla, and G. M. Burt, "Optimizing the Roles of Unit and Non-unit Protection Methods Within DC Microgrids," *IEEE Transactions on Smart Grid*, vol. 3, no. 4, pp. 2079-2087, Dec. 2012.
  - [25] R. Li, L. Xu, and L. Yao, "DC Fault Detection and Location in Meshed Multiterminal HVDC Systems Based on DC Reactor Voltage Change Rate," *IEEE Transactions on Power Delivery*, vol. 32, no. 3, pp. 1516-1526, June 2017.
  - [26] S. Dhar, R. K. Patnaik, and P. K. Dash, "Fault Detection and Location of Photovoltaic Based DC Microgrid Using Differential Protection Strategy," *IEEE Transactions on Smart Grid*, vol. 9, no. 5, pp. 4303-4312, Sept. 2018.
  - [27] S. P. Gao, Q. Liu, and G. B. Song, "Current differential protection principle of HVDC transmission system," *IET Generation, Transmission & Distribution*, vol. 11, no. 5, pp. 1286-1292, March 2017.
  - [28] S. D. A. Fletcher, P. J. Norman, K. Fong, S. J. Galloway, and G. M. Burt, "High-Speed Differential Protection for Smart DC Distribution Systems," *IEEE Transactions on Smart Grid*, vol. 5, no. 5, pp. 2610-2617, Sept. 2014.
  - [29] R. M. Cuzner, and V. Singh, "Future Shipboard MVdc System Protection Requirements and Solid-State Protective Device Topological Tradeoffs," *IEEE Journal of Emerging and Selected Topics in Power Electronics*, vol. 5, no. 1, pp. 244-259, March 2017.
  - [30] National Instruments (2017). How to Measure Voltage, Current, and Power. [Online]. Available: <http://www.ni.com/white-paper/8198/en/>
  - [31] A. Hooshyar, and M. Sanaye-Pasand, "Accurate Measurement of Fault Currents Contaminated With Decaying DC Offset and CT Saturation," *IEEE Transactions on Power Delivery*, vol. 27, no. 2, pp. 773-783, April 2012.
  - [32] X. Tian, and R. Moussanet, "Current measurement using switch voltage drop in IGBT DC circuit breaker application," in *Proc. 5th European Conference on Power Electronics and Applications 1993*, 1993, vol.2, pp. 332-336, Sep. 1993.
  - [33] C. Yuan, M. A. Haj-ahmed, and M. S. Illindala, "Protection Strategies for Medium-Voltage Direct-Current Microgrid at a Remote Area Mine Site," *IEEE Transactions on Industry Applications*, vol. 51, no. 4, pp. 2846-2853, July-Aug. 2015.
  - [34] K. Satpathi, N. Thukral, A. Ukil, and M. A. Zagrodnik, "Directional protection scheme for MVDC shipboard power system," in *Proc. 42nd Annual Conference of the IEEE Industrial Electronics Society (IECON) 2016*, Florence, pp. 3840-3847, Oct. 2016.
  - [35] D. Jovicic, M. Taherbaneh, J. P. Taisne, and S. Nguefeu, "Offshore DC Grids as an Interconnection of Radial Systems: Protection and Control Aspects," *IEEE Transactions on Smart Grid*, vol. 6, no. 2, pp. 903-910, March 2015.
  - [36] G. Wawrzola, "Challenges of DC Data Center Power Distribution Protection," in *Proc. 13th International Conference on Development in Power System Protection (DPSP) 2016*, pp. 1-6, Mar. 2016.
  - [37] J. Yang, J. E. Fletcher and J. O'Reilly, "Short-Circuit and Ground Fault Analyses and Location in VSC-Based DC Network Cables," *IEEE Transactions on Industrial Electronics*, vol. 59, no. 10, pp. 3827-3837, Oct. 2012.
  - [38] H. Li, M. Chen, B. Yang, F. Blaabjerg and D. Xu, "A fast fault protection based on direction of bus-side capacitor discharge current for a high-surety power supply," in *Proc. IEEE Energy Conversion Congress and Exposition (ECCE) 2017*, Cincinnati, pp. 542-549, Oct. 2017.



**Haijin Li** (S'13) received the B.S. degree in electrical engineering from the Department of Electrical Engineering, Zhejiang University, Hangzhou, China, in 2010, where he is currently working toward the Ph.D. degree. He was supported by the China Scholarship Council to visit and work in Department of Energy Technology, Aalborg University, Denmark, from 2016 to 2017. His current research interests include protection and controls of multiple energy storage systems and DC microgrids.





**Min Chen** (M'06) received the B.S. and Ph.D. degrees in power electronics from the Department of Electrical Engineering, Zhejiang University, Hangzhou, China, in 1998 and 2004, respectively. He is currently Associate Professor of College of Electrical Engineering at Zhejiang University. His research interests include power quality control, high-frequency high-power conversion, and renewable energy power conversion system.



**Boping Yang** received the B.S. degree in electrical engineering from the Department of Electrical Engineering and Automation, Tianjin University, Tianjin, China, in 2013. He received the M.S. degree in power electronics from Department of Electrical Engineering, Zhejiang University, Hangzhou, China, in 2016. His research interests include wireless power transfer and protection of power electronics system.

Now he is a senior engineer in Huawei Technologies Co., Ltd.



**Frede Blaabjerg** (S'86–M'88–SM'97–F'03) was with ABB-Scandia, Randers, Denmark, from 1987 to 1988. From 1988 to 1992, he got the PhD degree in Electrical Engineering at Aalborg University in 1995. He became an Assistant Professor in 1992, an Associate Professor in 1996, and a Full Professor of power electronics and drives in 1998. From 2017 he became a Villum Investigator. He is honoris causa at University Politehnica Timisoara (UPT), Romania and Tallinn Technical University (TTU) in Estonia.

His current research interests include power electronics and its applications such as in wind turbines, PV systems, reliability, harmonics and adjustable speed drives. He has published more than 500 journal papers in the fields of power electronics and its applications. He is the co-author of two monographs and editor of 7 books in power electronics and its applications.

He has received 26 IEEE Prize Paper Awards, the IEEE PELS Distinguished Service Award in 2009, the EPE-PEMC Council Award in 2010, the IEEE William E. Newell Power Electronics Award 2014 and the Villum Kann Rasmussen Research Award 2014. He was the Editor-in-Chief of the IEEE TRANSACTIONS ON POWER ELECTRONICS from 2006 to 2012. He has been Distinguished Lecturer for the IEEE Power Electronics Society from 2005 to 2007 and for the IEEE Industry Applications Society from 2010 to 2011 as well as 2017 to 2018. In 2018 he is President Elect of IEEE Power Electronics Society.

He is nominated in 2014, 2015, 2016 and 2017 by Thomson Reuters to be between the most 250 cited researchers in Engineering in the world.



**Dehong Xu** (M'94–SM'09–F'13) received the B.S., M.S., and Ph.D. degrees from the Department of Electrical Engineering, Zhejiang University, Hangzhou, China, in 1983, 1986, and 1989, respectively.

Since 1996, he has been with the College of Electrical Engineering, Zhejiang University, China, as a Full Professor. He was a Visiting Scholar in the University of Tokyo, Japan, from June 1995 to May 1996. From June to December 2000, he was a Visiting Professor in CPES of Virginia Tech, USA. From

February 2006 to April 2006, he was a Visiting Professor in ETH, Switzerland. His current research interests include power electronics topology and control, power conversion for energy saving and renewable energy. He has authored or coauthored six books and more than 160 IEEE Journal or Conference papers. He owns more than 40 Chinese patents and 3 U.S. patents.

Dr. Xu is the recipient of four IEEE journal or conference paper awards. From 2013, He is the President of the China Power Supply Society. He is an At-Large Adcom Member of the IEEE Power Electronics Society from 2017 to 2019. He is an Associate Editor of the IEEE Transactions on Power Electronics. He is the IEEE PELS Distinguished Lecturer in 2015- 2017. In 2016, he received IEEE PELS R. D. Middlebrook Achievement Award.